Optical Switching Based on Polarization Tunable Plasmon-Induced Transparency in Disk/Rod Hybrid Metasurfaces

Jin-Na He · Jun-Qiao Wang · Pei Ding · Chun-Zhen Fan · Luk R. Arnaut · Er-Jun Liang

Abstract Dynamical control of plasmon-induced transparency (PIT) in metamaterials promises essential application opportunities. In this paper, we design a novel disk/rod hybrid metasurface to investigate an actively controlled PIT spectral response through polarization-dependent near-field coupling between the disk (bright) and the rod (dark) resonator. It is found that an on-to-off amplitude modulation of the PIT transparency window is achieved by the rotation of polarization, allowing for dynamically tunable group delays of incident waves. An analytic model based on the dipole-dipole interactions is developed for the proposed configuration, which agrees well with the numerical results. The disk/rod metasurface offers great promise for optical switching and compact slow light devices.

Keywords Disk/rod hybrid metasurface · Plasmon induced transparency · Polarization dependent near-field coupling · Optical switching · Slow light

J.-N. He · J.-Q. Wang · C.-Z. Fan · E.-J. Liang (✉)
School of Physical Science and Engineering and Key Laboratory of Materials Physics of Ministry of Education of China, Zhengzhou University, Zhengzhou 450052, People's Republic of China
e-mail: ejliang@zzu.edu.cn

J.-N. He
College of Electric and information Engineering, Pingdingshan University, Pingdingshan, Henan Province 467000, People's Republic of China

P. Ding
Department of Mathematics and Physics, Zhengzhou Institute of Aeronautical Industry Management, Zhengzhou 450015, People's Republic of China

L. R. Arnaut
School of Electronic Engineering and Computer Science, Queen Mary University of London, London E1 4FZ, UK

Introduction

Metamaterial has become a versatile platform in the field of integrated photonic devices due to unusual electromagnetic properties supported by engineered metallic structures with unit size much smaller than the wavelengths of radiation [1–3]. The most prominent feature is the freedom to be able to design the "meta-atoms" at will to achieve well-controlled optical properties not obtained in natural materials or mimicking optical properties occurring in natural materials but under quite stringent experimental conditions, such as Fano resonance [4–7] or electromagnetically induced transparency (EIT) in atomic three-level systems [8]. A metamaterial analogue of EIT, also called as plasmon-induced transparency (PIT), can be achieved simply by artificially designing a super-radiative (bright) resonator coupled with a sub-radiative (dark) resonator [9]. The coupling between a bright and a dark resonator results in the destructive interference between two excitation pathways of bright modes that gives rise to a spectrally narrow transmission window within a broad absorption background. Within this window, dramatically slowed down photons and significantly enhanced nonlinearities enable the manipulation of light at the energy levels corresponding to just a few photons [10], opening up possibilities for nonlinear optics and optical information processing. Now, many PIT metamaterial structures have been proposed, such as the symmetrical resonators of nanorod and the asymmetrical, simplified as well as complex resonators [11–15].

The ability to actively control PIT effects enables a dynamic tunability of group velocity of light and potentially extends the range of the applications even further, e.g., wireless optical communication and optical networks. Some schemes have been proposed to obtain actively controlled PIT in metamaterials [16–20]. However, they mostly depend on integrating

metamaterials with various active materials, such as quantum dots, semiconductors with the electrically/optically controlled free carriers, superconductor, or graphene. For example, Gu et al. demonstrated optically tunable PIT by integrating photoactive silicon into metamaterials, where the modulation mechanism is attributed to a change in the damping rates of dark modes caused by silicon under photoexcitations [16]. Jin et al. demonstrated the controlled PIT in metamaterials by adjusting incident angle based on the phase coupling [18]. Very few attempts are based on the active control of other physical parameters, including the coupling strength between two resonators, the damping rate of bright modes, and the detuning of resonant frequency of bright modes from dark modes.

In this paper, we proposed a novel disk/rod hybrid metasurface that supports PIT resonance without breaking structural symmetry. The directly excited dipolar resonance in disk is coupled to the quadrupolar resonance of the rod via localized electric fields produced at the gap between them, leading to an obvious PIT transparency window in the visible frequency. Interestingly, an on-off modulation of the PIT transparency window can be achieved by the rotation of polarization of the excitation light. Moreover, a simple analytical model based on classical dipole-dipole interactions is developed for the structure, which quantitatively and intuitively explains the polarization-dependent PIT phenomenon.

Structure Design and Simulation Method

The target focused in this paper is a two-dimensional periodic array of the disk/rod hybrid nanostructure with the period of 500 nm smaller than the incident wavelengths, that is, a plasmonic metasurface. Figure 1 displays the schematic of the unit cell of the metasurface, consisting of a disk and a long rod. The diameter of the disk is $D=240$ nm. The length and width of the long rod are $L=310$ nm and $W=40$ nm, respectively. The thickness of the disk and the rod is $H=20$ nm, and the edge-to-edge gap width between the disk and the rod is $g=30$ nm. Numerical simulations are carried out by finite element method (FEM) with COMSOL Multiphysics. The
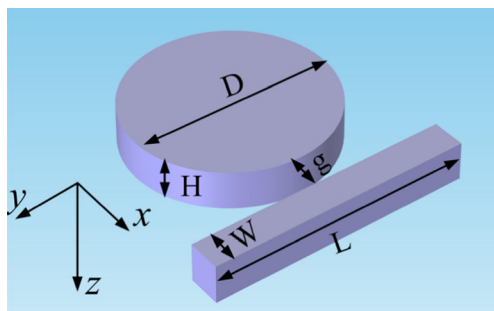
computation domain consists of a unit cell, where perfectly matched layers (PML) are applied along the boundaries normal to the propagation direction (z-axis), and periodic conditions are employed to four lateral boundaries in x- and y-directions. Silver is chosen as the disk and rod material due to its low intrinsic damping, whose frequency-dependent permittivity is described by Drude model with the plasma frequency $\omega_p=1.366\times10^{16}$ rad/s and the damping constant $\gamma=3.07\times10^{13}$ 1/s [9, 21].

Results and Discussions

Figure 2a shows the transmission spectrum of the disk/rod metasurface at normal incidence with the E-field polarization along x-axis. As a reference, the transmissions of the solely disk and rod array are also given. It is found that the disk array exhibits a typical Lorentz line-shaped resonance arising from the radiative dipolar plasmon mode of the disk. By contrast, under the same excitation conditions, the rod array shows no response because the polarization of excitation light is normal to its long axis. The geometrical parameters of the rod have been optimized to ensure its quadrupole mode resonant at the same frequency as the disk's dipole mode (420 THz) by calculating its optical response at oblique incidence. The quadrupole mode can be excited by an adjacent dipolar source [22].
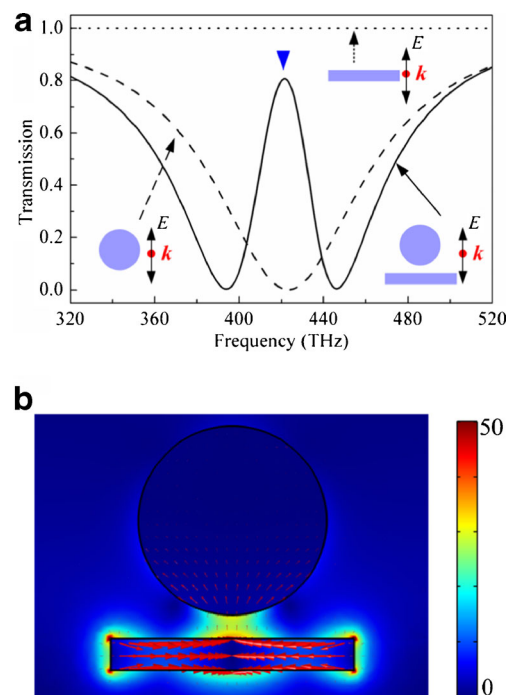

Fig. 2 **a** Transmission spectra of the solely disk array, the solely rod array and the disk/rod hybrid array. *Inset*: E indicates incident E-polarization direction, and k shows incident direction. **b** Distributions of the electric fields (|E|) and current density (J) at PIT frequency (420 THz). The *arrows* represent the directions of current oscillations

Fig. 1 Schematic of the unit cell of the disk/rod metasurface, where the geometrical parameters D, H, W, L and g are defined

Thus, when both resonators are arranged in close proximity to each other, the dipolar resonance in disk excited directly by incident light acts as a point source and couples to the quadrupolar mode in the rod through the near-field interactions. As a result, the bright mode in disk can be excited in two pathways: |I⟩→|B⟩ and |I⟩→|B⟩→|D⟩→|B⟩, with |I⟩, |B⟩, and |D⟩ representing incident source, bright, and dark modes, respectively. The two pathways interferences destructively, resulting in the suppression of polarization of the bright mode and a corresponding transparency band instead of the original transmission dip. As illustrated in Fig. 2b, the polarization of the disk is suppressed and the quadrupole mode with three nodes of electric fields in the rod is observed obviously.

The amplitude modulation of the PIT transparency peak is observed clearly by rotating the polarization orientations of excitation light, as shown in Fig. 3a. The angle of the polarization direction with respect to the x-axis is defined as θ (See the inset). In the case of θ=0°, a pronounced transparency peak with a transmittance of about 85 % appears between at two resonant dips. With increasing θ, the transparency peak gradually shrinks without a notable frequency shift. If θ is increased further to 90°, the PIT spectral feature disappears completely, leaving only a single transmission dip with the transmittance as low as 10 % in the transmission spectrum. In this case, the transmission spectrum is very similar to that of the solely disk array shown in Fig. 2a.

In order to get into the underlying physics of the polarization-tunable PIT behavior, the distributions of electric fields at the spectral position of one of dips, as denoted by red arrow in Fig. 3a, are shown in Fig. 3b for different polarization angles. Here, the transmission dip instead of the peak is chosen for simultaneously displaying the disk's polarization (bright mode) since it is suppressed at the PIT frequency. Because the disk and the rod are coupled as the bonding mode, a prominent field enhancement is produced at the gap between the disk and rod for the low-frequency dip. On the contrary, the electric fields at the gap are suppressed greatly for another transmission dip (at the high frequency) due to the formation of the anti-bonding mode, which is not shown here. From Fig. 3b, it is revealed that for θ=0°, an electric dipole in disk driven by the incident polarization is coupled to the rod's electric quadrupole via the localized electric fields produced at the gap vicinity. With the increase of θ, the polarization direction of the dipole in disk is changed consistently along with the incident polarization, whereas the quadrupolar mode in rod is independent of the polarization angle due to its dark feature and oscillates always parallel with the long symmetry axis of the rod. Actually, as θ is increased, the effective coupling angular separation between the disk and the rod is enlarged, causing the near-field coupling between bright and dark modes to weaken. Accordingly, the PIT resonance becomes increasingly not pronounced and disappears at θ=90°, where the near-field coupling is suppressed, and only a single dipole resonance of the disk exists. The central frequency of the PIT resonance nearly keeps constant during this process due to the structural isotropy of the disk. A small blueshift of the central frequency with respect to the case of θ=0° is attributed to the longitudinal interaction between the disk and rod. If the gap distance g is enlarged, the blueshift will disappear.

The near-field coupling between the two resonators can be evaluated by the E-field intensity at the position of the gap center (See the inset of Fig. 4a). The E-field intensity is obtained by placing a virtual E-field probe at this position, and the results are shown as a function of θ in Fig. 4a. At θ=0°, the E-field intensity (|E|) is the largest, indicating a large coupling strength. With the increase of θ, the E-field intensity decreases markedly and finally reaches a value of less than 1 at θ=90°. Obviously, the near-field coupling between the disk and the rod is significantly reduced with increasing the polarization angle, which contributes to a giant amplitude modulation of the PIT resonance.

The classical dipole-dipole interaction is a simple electrostatic model from which we can directly derive the interaction
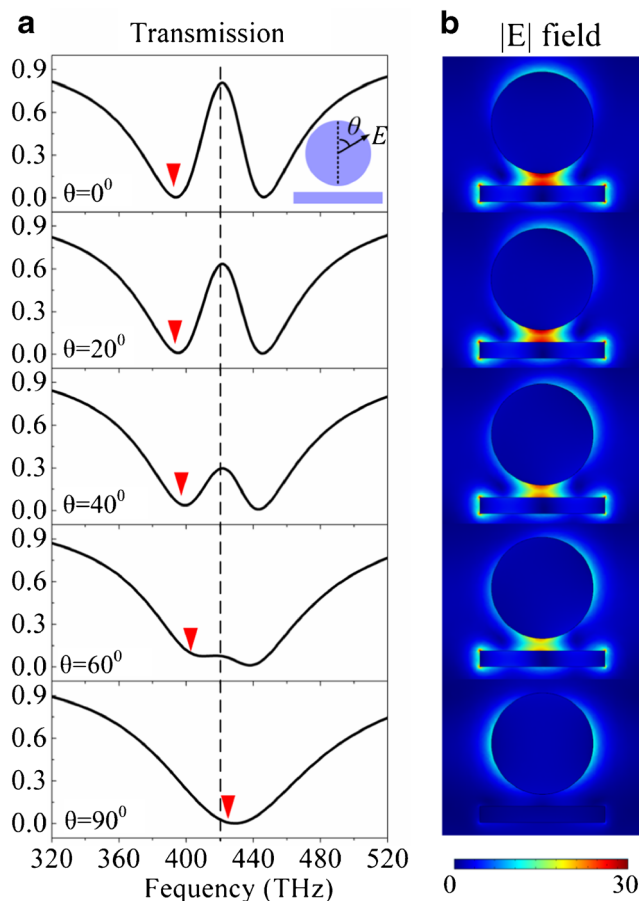

Fig. 3 **a** Transmission spectra of the disk/rod metasurface at different polarization angle θ. *Vertical dashed line* indicates the central frequency of PIT resonance. **b** Electric field (|E|) distributions at the dip spectral positions, which are denoted by *red arrows* in **a**
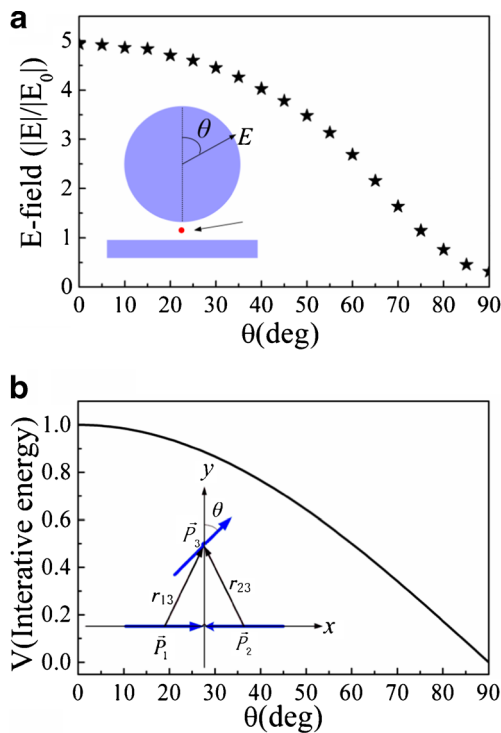
Fig. 4 **a** E-field enhancements located at the gap center (indicated by a *red dot* in the *inset*) for the low-frequency transmission dip as a function of the polarization angle θ. **b** Theoretical results of interactive energy between the dipole and the quadrupole mode as a function of θ. The *inset* is an analogy of the polarized states of the disk/rod hybrid system induced by excitation light. The dipole $\vec{P}_3$ represents the dipolar resonance of the disk, while the two identical collinear anti-parallel dipoles $\vec{P}_1$ and $\vec{P}_2$ represents the quadrupolar mode of the rod

energy between two coupled plasmon resonators [23]. In order to provide an intuitive theoretical picture of the polarization-dependent near-field coupling between disk and rod, an analytic expression is developed for the proposed configuration base on this model. As shown in inset of Fig. 4b, the dipole resonance in the disk is represented by an electric dipole $\vec{P}_3$, while the linear quadrupole resonance in the rod can be viewed as the combination of two identical collinear anti-parallel electric dipoles $\vec{P}_1$ and $\vec{P}_2$. In the quasi-static approximation, the interactive energy V between the disk's dipole mode and the rod's quadrupole mode can be expressed as the linear sum of both dipole-dipole mutual energies [24, 25]:

$$V = V_{13} + V_{23} = \frac{-3}{4\pi\varepsilon_0}\left(\frac{\left(\vec{P}_1\cdot\vec{r}_{13}\right)\left(\vec{P}_3\cdot\vec{r}_{13}\right)}{r_{13}^5} + \frac{\left(\vec{P}_2\cdot\vec{r}_{23}\right)\left(\vec{P}_3\cdot\vec{r}_{23}\right)}{r_{23}^5}\right) \quad (1)$$

where $\vec{r}_{13}$ and $\vec{r}_{23}$ are the center-to-center distance vectors directed from $\vec{P}_1$ to $\vec{P}_3$ and $\vec{P}_2$ to $\vec{P}_3$, respectively. Because

the electric dipole $\vec{P}_3$ is just located at the symmetry axis of the quadrupole mode, the interactive energy is thus simplified as follows:

$$V = \frac{-3}{4\pi\varepsilon_0}\left(\frac{\left(\vec{P}_1\cdot\vec{r}_{13}\right)\left|\vec{r}_{13} + \vec{r}_{23}\right|P_3\cos(\theta)}{r_{13}^5}\right) \quad (2)$$

From Eq. 2, we can conclude that, when the polarization angle θ is 0°, the interactive energy V is the largest. With the increase of θ along with the polarization of excitation light, the interactive energy V becomes weaker and weaker. When the polarization angle θ is 90°, the interactive energy V approaches zero. It is revealed further in theory that the evolution process of the PIT transmission spectra in dependence on the polarization angle arises from a change in the coupling strength between the disk's dipole mode and the rod's quadrupole mode. The theoretical result using the dipole-quadrupole interaction model (Fig. 4b) exhibits a good agreement with the FEM numerical simulation result (Fig. 4a).

Besides the polarization angle, the interactive energy V also depends on the relative distance between the dipole and the quadrupole mode from Eq. 2. A smaller distance corresponds to a larger interactive energy. This indicates that the PIT resonance can also be affected by changing the gap distance g. Figure 5 shows the transmission spectra of the disk/rod metasurface with different g. It is found that as g decreases, the transparency window grows in strength and becomes more and more prominent due to the increase of the coupling strength (that is, the interactive energy) from Eq. 2. For g less than 20 nm, the center frequency of the PIT peak, especially the low-frequency dip, produces an obvious red shift. This tunability based on altering the relative distance between the resonators has been demonstrated widely in previous work. However, it is not desirable from the viewpoint of practical applications because this tunability will disappear once the samples are fabricated (passive control).
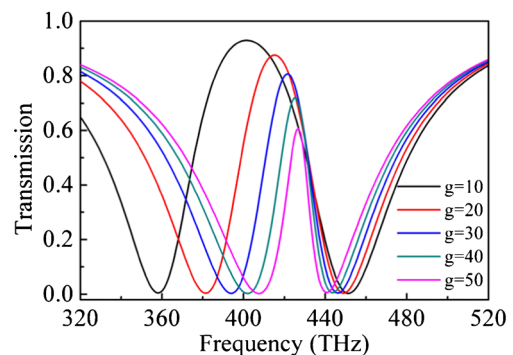

Fig. 5 Transmission spectra of the disk/rod metasurface with different gap distance (in nanometer). The incident polarization is along x-axis (θ=0°)

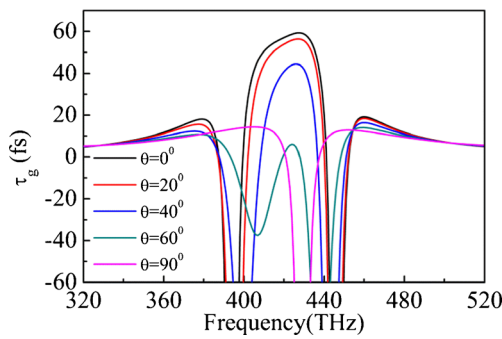**Fig. 6** Group delays for various polarization angles. Here, $\tau_g = \tau_g^{EIT} - \tau_g^{air}$, where τ_g^{EIT} and τ_g^{air} are the group delays through an air box with and without the disk/rod hybrid metasurface, respectively

One important character of the PIT effects is to support the slow light propagation [26–28]. To demonstrate the capability of slowing light, the group delay (τ_g) of incident light through

the disk/rod metasurface is estimated according to the following formula [29]:

$$\tau_g = \tau_g^{EIT} - \tau_g^{air} = -\left(\frac{d\varphi_{EIT}(\omega)}{d\omega} - \frac{d\varphi_{air}(\omega)}{d\omega} \right) \qquad (3)$$

where τ_g^{EIT} and τ_g^{air} are the group delays through an air box with and without the disk/rod metasurface when the gap $g=$ 20 nm, and φ_{EIT} and φ_{air} are the phases of the respective transmitted wave in these two cases. Figure 6 shows the group delay spectra under various polarization angles. It can be seen that the group delay time is about 60 fs at PIT frequency for $\theta=0°$, which is equivalent to a time delay for the free space propagation across a 18-μm distance. The capability of slowing light is noteworthy, because the actual thickness of the metasurface is very thin and only 20 nm. When the
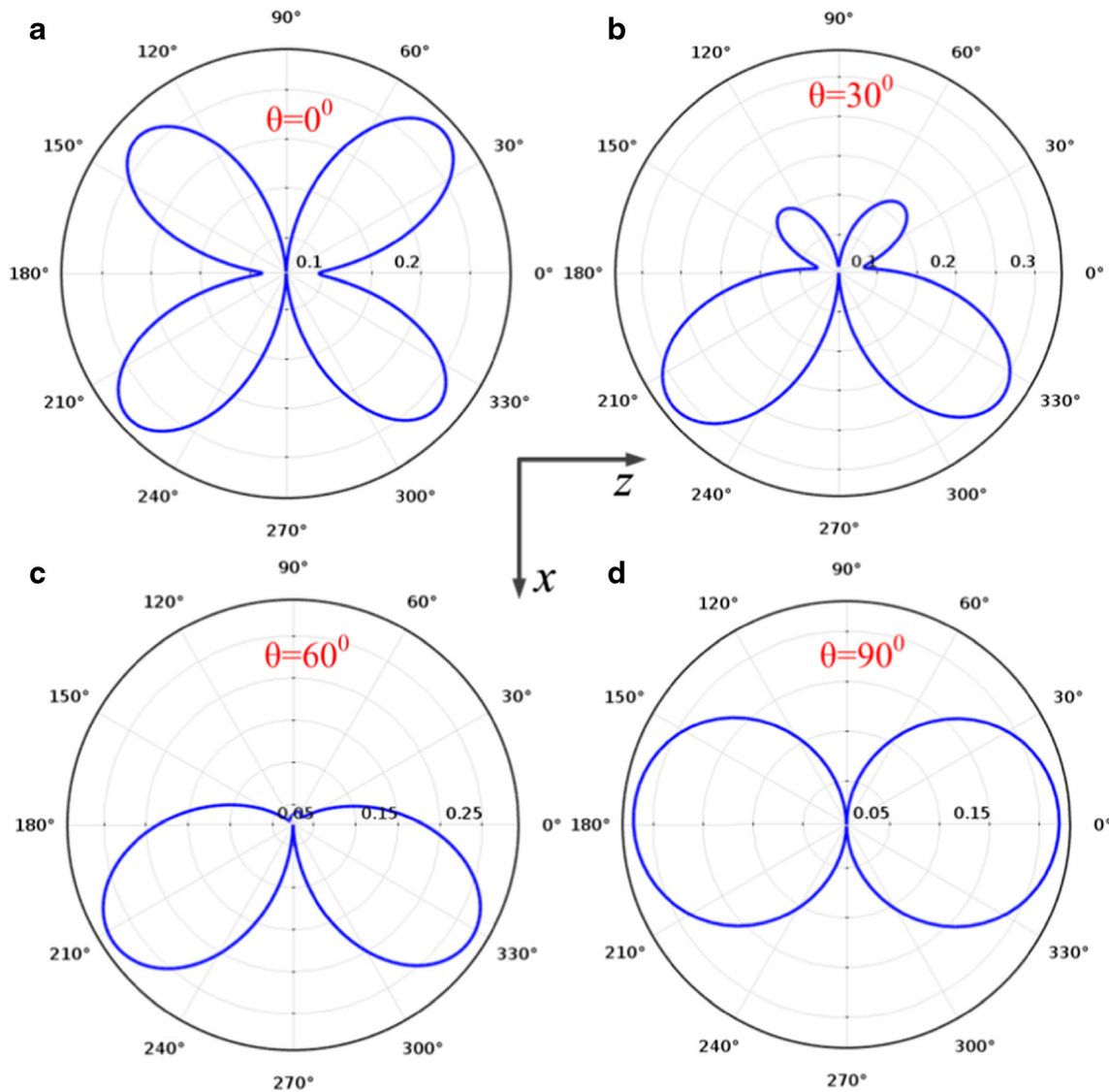

Fig. 7 Patterns of the scattered light in the far field for the disk/rod metasurface in *x-z* plane at different polarization angles, **a** $\theta=0°$, **b** 30°, **c** 60°, and **d** 90°. The frequency is chosen to be 420 THz corresponding to the PIT resonance

polarization angle is increased gradually, the slow light characteristic is weakened obviously and finally lost at $\theta=90°$, where it is turned into a typical group-delay characteristic of localized surface plasmon resonances. The active, giant modulation of the group delays of optical wave by the incident polarization makes this geometry promising for application in compact slow light devices.

Finally, we investigate the influence of rotation of the polarization on the angular distribution of the scattered light in the far-field for the disk/rod hybrid metasurface. Figure 7 displays the scattering pattern in the x-z plane at the PIT frequency (420 THz), which depends sensitively on the polarization orientations of the excitation light. At $\theta=0°$, the scattering pattern presents four lobes at nearly right angles from each other, with a symmetrical angular distribution around the x-axis. It corresponds to a linear quadrupole mode arising from the long metal rod [30], which is excited by the disk's dipole resonance through the near-field interactions. With increasing θ, the quadrupole resonance becomes weaker and weaker due to decreased near-field coupling, resulting in the transition of the scattering pattern gradually from the quadrupole to the dipole radiation, as displayed in Fig. 7b, c. Finally, the scattering pattern of a dipole mode arising from the disk is observed at $\theta=90°$ when the near-field interactions between the disk and the rod is suppressed, and the PIT effect disappears completely.

Conclusions

In summary, we have theoretically demonstrated the PIT spectral response in a disk/rod hybrid metasurface. With the aid of the polarization-dependent near-field coupling, on-off switching of the PIT transparency window is achieved by rotating the polarization from 0° to 90°. Based on this observed phenomenon, an optical switching function can be realized. Besides, the polarization-dependent group delays and scattering patterns in far field have also been demonstrated. The metasurface has great promise for a wide range of applications in compact optical components and nonlinear devices. In addition, it may inspire interest in developing dynamically tunable PIT metasurface with an applied voltage if placed into active mediums such as liquid crystal.

References

1. Pendry JB, Holden AJ, Robbins DJ, Stewart WJ (1999) Magnetism from conductors and enhanced nonlinear phenomena. IEEE Trans Microwave Theory Tech 47(11):2075–2084
2. Smith DR, Pendry JB, Wiltshire MCK (2004) Metamaterials and negative refractive index. Science 305(5685):788–792
3. Valentine J, Zhang S, Zentgraf T, Ulin-Avila E, Genov DA, Bartal G, Zhang X (2008) Three-dimensional optical metamaterial with a negative refractive index. Nature 455:376–379
4. Fedotov VA, Rose M, Prosvirnin SL, Papasimakis N, Zheludev NI (2007) Sharp trapped-mode resonances in planar metamaterials with a broken structural symmetry. Phys Rev Lett 99:147401
5. Wu C, Arju N, Kelp G, Fan JA, Dominguez J, Gonzales E, Tutuc E, Brener I, Shvets G (2014) Spectrally selective chiral silicon metasurfaces based on infrared Fano resonances. Nat Commun 5:3892
6. Argyropoulos C, Monticone F, D'Aguanno G, Alu A (2013) Plasmonic nanoparticles and metasurfaces to realize Fano spectra at ultraviolet wavelengths. Appl Phys Lett 103:143113
7. Cao W, Singh R, Al-Naib I, Ibraheem A, He M, Taylor AJ, Zhang W (2012) Low-loss ultra-high-Q dark mode plasmonic Fano metamaterials. Opt Lett 37:3366–3368
8. Harris SE (1997) Electromagnetically induced transparency. Phys Today 50(7):36–42
9. Zhang S, Genov DA, Wang Y, Liu M, Zhang X (2008) Plasmon-induced transparency in metamaterials. Phys Rev Lett 101:047401
10. Harris S, Field J, Imamoğlu A (1990) Nonlinear optical processes using electromagnetically induced transparency. Phys Rev Lett 64:1107
11. Liu N, Langguth L, Weiss T, Kästel J, Fleischhauer M, Pfau T, Giessen H (2009) Plasmonic analogue of electromagnetically induced transparency at the Drude damping limit. Nat Mater 8:758–762
12. Liu X, Gu J, Singh R, Ma Y, Zhu J, Tian Z, He M, Han J, Zhang W (2012) Electromagnetically induced transparency in terahertz plasmonic metamaterials via dual excitation pathways of the dark mode. Appl Phys Lett 100:131101
13. Zhang K, Wang C, Qin L, Peng RW, Xu DH, Xiong X, Wang M (2014) Dual-mode electromagnetically induced transparency and slow light in a terahertz metamaterial. Opt Lett 39:3539–3543
14. Shao J, Li J, Li J, Wang YK, Dong ZG, Chen P, Wu RX, Zhai Y (2013) Analogue of electromagnetically induced transparency by doubly degenerate modes in a U-shaped metamaterial. Appl Phys Lett 102:034106
15. Miyata M, Hirohata J, Nagasaki Y, Takahara J (2014) Multi-spectral plasmon induced transparency via in-plane dipole and dual-quadrupole coupling. Opt Express 22:11399–11406
16. Gu J, Singh R, Liu X, Zhang X, Ma Y, Zhang S, Maier SA, Tian Z, Azad AK, Chen HT (2012) Active control of electromagnetically induced transparency analogue in terahertz metamaterials. Nat Commun 3:1151
17. Chowdhury DR, Singh R, Taylor AJ, Chen HT, Azad AK (2013) Ultrafast manipulation of near field coupling between bright and dark modes in terahertz metamaterial. Appl Phys Lett 102:011122
18. Jin XR, Lu Y, Park J, Zheng H, Gao F, Lee Y, Rhee JY, Kim KW, Cheong H, Jang WH (2012) Manipulation of electromagnetically-induced transparency in planar metamaterials based on phase coupling. J Appl Phys 111:073101
19. Lu Y, Rhee JY, Jang WH, Lee YP (2010) Active manipulation of plasmonic electromagnetically-induced transparency based on magnetic plasmon resonance. Opt Express 18:20912–20917
20. Miyamaru F, Morita H, Nishiyama Y, Nishida T, Nakanishi T, Kitano M, Takeda MW (2014) Ultrafast optical control of group delay of narrow-band terahertz waves. Sci Rep 4:4346
21. Jin XR, Park J, Zheng H, Lee S, Lee Y, Rhee JY, Kim KW, Cheong H, Jang WH (2011) Highly-dispersive transparency at optical frequencies in planar metamaterials based on two-bright-mode coupling. Opt Express 19:21652–21657

22. Yang ZJ, Zhang ZS, Zhang LH, Li QQ, Hao ZH, Wang QQ (2011) Fano resonances in dipole-quadrupole plasmon coupling nanorod dimers. Opt Lett 36:1542–1544

23. Rechberger W, Hohenau A, Leitner A, Krenn JR, Lamprecht B, Aussenegg FR (2003) Optical properties of two interacting gold nanoparticles. Opt Commun 220:137–141

24. Jackson JD (1975) Classical electrodynamics. John Wiley & Sons, New York

25. Liu N, Giessen H (2010) Coupling effects in optical metamaterials. Angew Chem Int Ed 49:9838–9852

26. Tassin P, Zhang L, Koschny T, Economou E, Soukoulis CM (2009) Low-loss metamaterials based on classical electromagnetically induced transparency. Phys Rev Lett 102:053901

27. Liu SD, Yang Z, Liu RP, Li XY (2011) Plasmonic-induced optical transparency in the near-infrared and visible range with double split nanoring cavity. Opt Express 19:15363–15370

28. Wang J, Yuan B, Fan C, He J, Ding P, Xue Q, Liang E (2013) A novel planar metamaterial design for electromagnetically induced transparency and slow light. Opt Express 21:25159–25166

29. Zentgraf T, Zhang S, Oulton RF, Zhang X (2009) Ultranarrow coupling-induced transparency bands in hybrid plasmonic systems. Phys Rev B 80:195415

30. Encina ER, Coronado EA (2008) Plasmonic nanoantennas: angular scattering properties of multipole resonances in noble metal nanorods. J Phys Chem C 112:9586–9594